

Comparing satellite SAR and wind farm wake models

CB Hasager^{1a}, P Vincent^b, R Husson^b, A Mouche^c, M Badger^a, A Peña^a, P Volker^a, J Badger^a, A Di Bella^a, A Palomares^d, E Cantero^e, PMF Correia^e

^aDTU Wind Energy, Frederiksborgvej 399, 4000 Roskilde, Denmark

^bCLS, Avenue La Pérouse, Bâtiment le Ponant, 29280 Plouzané, France

^cIFREMER, Pointe du Diable, 29280 Plouzané, France

^dCIEMAT, Avenida Complutense 40, 28040 Madrid, Spain

^eCENER, Avda Ciudad de la Innovación 7, 31621 Sarriguren (Navarra), Spain,

E-mail: cbha@dtu.dk; pvincent@cls.fr; romain.husson@cls.fr; alexis.mouche@ifremer.fr; mebc@dtu.dk; aldi@dtu.dk; pvol@dtu.dk; jaba@dtu.dk; adia@dtu.dk; ana.palomares@ciemat.es; ecantero@cener.com; pmfernandez@cener.com

Abstract. The aim of the paper is to present offshore wind farm wake observed from satellite Synthetic Aperture Radar (SAR) wind fields from RADARSAT-1/-2 and Envisat and to compare these wakes qualitatively to wind farm wake model results. From some satellite SAR wind maps very long wakes are observed. These extend several tens of kilometres downwind e.g. 70 km. Other SAR wind maps show near-field fine scale details of wake behind rows of turbines. The satellite SAR wind farm wake cases are modelled by different wind farm wake models including the PARK microscale model, the Weather Research and Forecasting (WRF) model in high resolution and WRF with coupled microscale parametrization.

1. Introduction

The wake of the offshore wind farms are observed from Synthetic Aperture Radar (SAR) satellite data [1, 2, 3]. In the present study SAR data are extracted from the Canadian RADARSAT-1/-2 satellites and the European Space Agency satellite Envisat. The basic measurement principle consists of emitted microwave radiation at C-band (wavelength around 5 cm) that is backscattered from the natural surface and objects herein. For natural ocean surface it is the wind field dominating the backscatter but also ocean current, natural slicks from algae and oil seepage may influence backscatter. Furthermore, ocean swell waves, tidal flow over shallow water areas and sea ice produce imprint. The ocean objects observed are ships, wind turbines, oil/gas platforms and other man-made structures at sea. For the ocean surface, the roughness of the sea appears darker for lower wind speed and brighter for higher wind speed because the backscatter from capillary and short-gravity waves at the surface of the ocean relates to surface wind speed. More wind produces more short waves. Small white dots seen in SAR images over the ocean are most likely ships or wind turbines. The backscatter is very high for hard targets [4].

¹ To whom any correspondence should be addressed.



The investigation on wind farm wake is based on high-resolution SAR satellite data as this data source provides interesting overview of one or several wind farms at a specific time, i.e. the few seconds of observations while the satellite orbits above the area. The observed backscatter images may be processed into wind speed maps. The wind speed is retrieved from SAR using a geophysical model function (GMF) and with a priori input of wind direction information as well as information on the viewing angle geometry and azimuth angle [5].

This paper presents three cases where wakes are captured in SAR images. The wake modelling undertaken in the study includes the PARK microscale model [6] for the first case while the WRF mesoscale model [7] coupled to microscale parametrization is used for the second case. These results are from DTU. WRF is operated at high spatial resolution at CENER and CIEMAT and here used for the third case. The comparison of observed wind farm wake and model results is qualitative.

2. Wake case at Horns Rev 2 with fine-scale structure

The first wind farm wake case considered is from Horns Rev 2 in the Danish North Sea observed at 3 August 2011 at 09:49 UTC. The roughness image is shown in Figure 1.

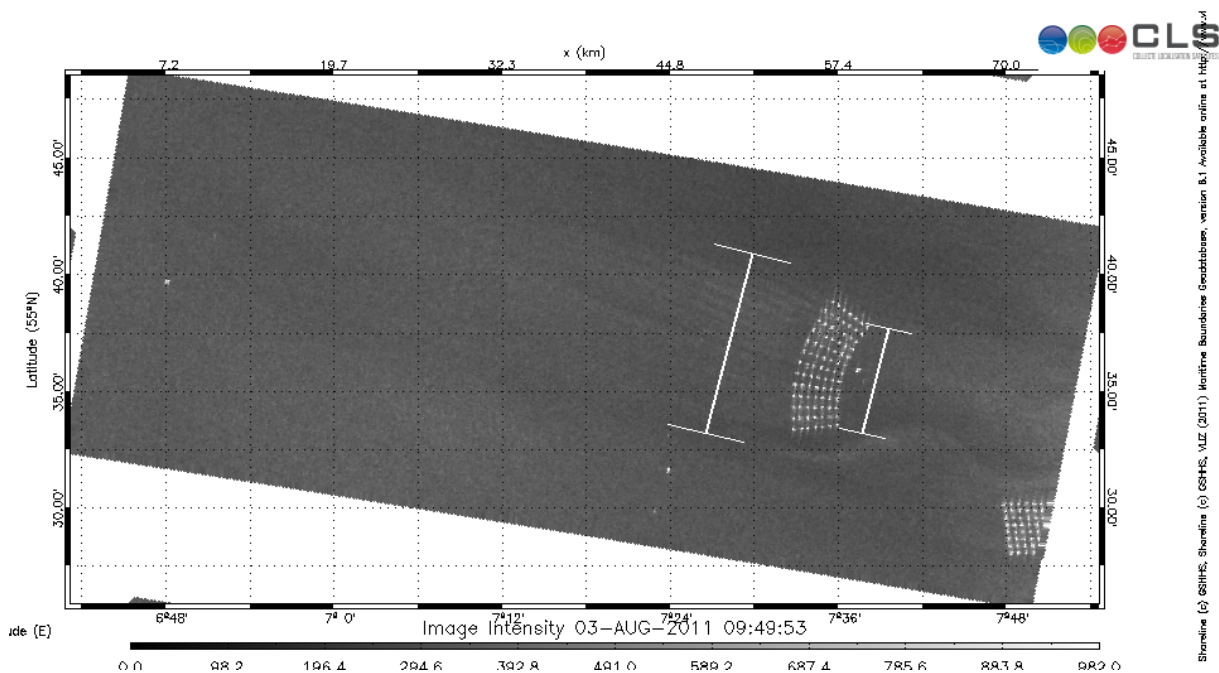


Figure 1. The roughness map is observed from Envisat ASAR IMG. The wind direction is from the east-southeast. Two horizontal transect lines are included upwind and downwind of Horns Rev 2.

In Figure 2 is shown the Normalized Radar Cross Section (NRCS) in dB along the horizontal transect west (downwind) of the wind farm while the NRCS along the upwind transect is shown in Figure 3. The polarization is horizontal transmit and receive (HH). From the SAR image the wake direction has been estimated at 111° and using this input for wind direction, wind speed has been retrieved using CMOD-IFR2 [8] and using polarization ratio 2 of [9]. The calculated equivalent neutral wind value is presented in Figure 2 and 3 for the downwind and upwind transects, respectively.

Looking at Figure 1 the wind farm wake is observed as fine-scale linear features aligned with the rows of wind turbines. The wake is most clearly visible in the northern half of the wind farm wake region.

In the downwind transect shown in Figure 2 the NRCS varies in a systematic pattern with up to 1 dB variation at very short distance. The retrieved wind speed shows variations from 4.8-6.0 ms^{-1} . Very interestingly the upwind horizontal transect shows wind speed values around 4.4 ms^{-1} with much smaller variation (around 0.3 ms^{-1}). The small variation in the upwind transect is most likely due to the natural uncertainty in the SAR data (so-called speckle noise) while the larger variation in the downwind transect most likely is due to influence from the wind turbines. It may also be noticed that there is speed up effect from the upwind to downwind transect. Speed up for winds blowing offshore is well-known [10].

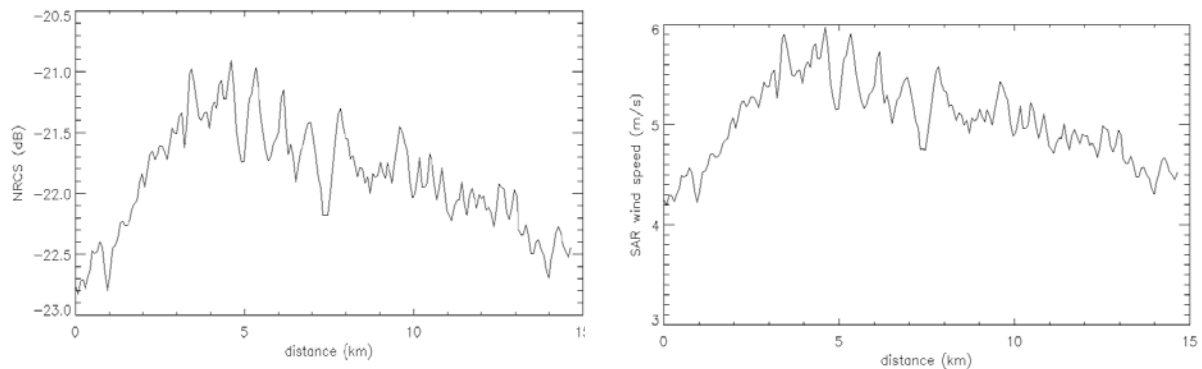


Figure 2. Horizontal transect from Figure 1. It is 15 km long and located downwind of the wind farm: (left) NRCS observed in the roughness map; (right) the wind speed retrieved from CMOD-IFR2.

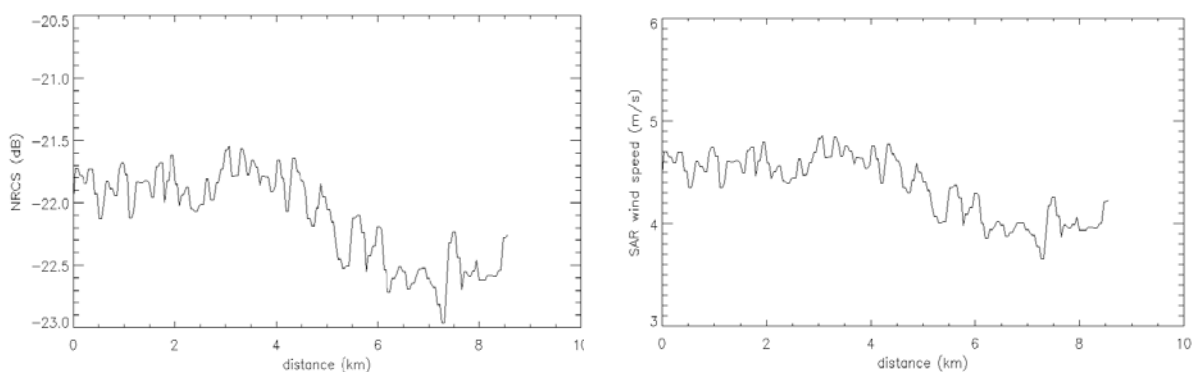


Figure 3. Horizontal transect from Figure 1. It is 8 km long and located upwind of the wind farm: (left) NRCS observed in the roughness map; (right) the wind speed retrieved from CMOD-IFR2.

To investigate the case further, the PARK microscale wake model has been used to assess the case. Figure 4 shows the map with position of wind turbines and results from PARK along the transect. The wind speed is near cut-in. The variation in wind speed behind the nearest turbines and between the rows is variable from 5.7-6.0 ms^{-1} in a regular pattern. This compare well to the observed wind speed variation in Figure 2. It is of course not obvious what ‘free stream’ wind speed value to use if the wind farm wake velocity deficit should be calculated, as the upwind wind speed is not constant along the wind direction due to coastal speed up effects. The ‘free stream’ wind speed observed north or south of the downwind transect vary from 4.2-4.5 ms^{-1} . In summary, the PARK model reproduces the fine-scale wind farm wake features observed in SAR. From the modelling point of view the challenges are that there is a clear coastal wind speed gradient and the flow is not homogeneous at the time of observation. Finally, it may be noted that in Figure 1 between Horns Rev 1 and 2 wind farms, a wavy large scale bright area is seen. This could be wake or it could be due to ocean current and bathymetry

effects at the shallow areas of the Horns Rev. Thus care should be taken in the interpretation of this bright area to have higher wind speed than the local areas nearby with darker tones.

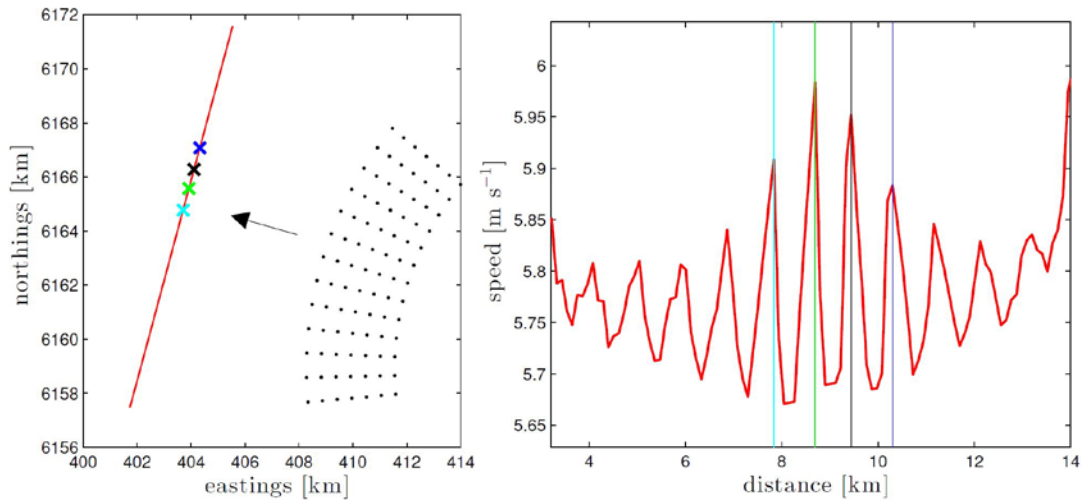


Figure 4. (left) The map of wind turbines at Horns Rev 2 and transect with four points highlighted. (right) the wake results from PARK along the transect with the four points indicated.

3. Wake case at Belwind1 and Thornton Bank with very long wakes

At the offshore wind farms Belwind1 and Thornton Bank 1+2+3 in the Belgium North Sea, two very long wind farm wakes, 79 and 65 km, respectively, were observed by an acquisition from RADARSAT-2 on the 1st of July of 2013 at 17:34 UTC. The flow is from the southwest. Figure 5 shows the intensity of the radar return signal and wind speed. The retrieved SAR wind map using CMOD-IFR2 is presented in Figure 6. This map clearly shows the wind deficit in the wind farms wake regions. The wind speed in the free stream region compared to the wake regions vary up to 1.5 m s^{-1} from $5.0\text{-}6.5 \text{ m s}^{-1}$. The wakes turns possible due to Coriolis effects, roughness changes and mesoscale meandering.

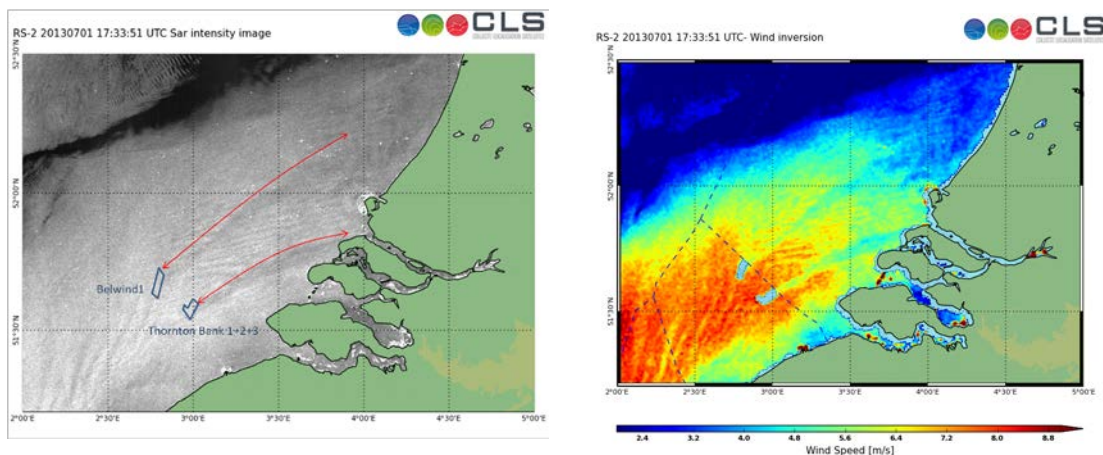


Figure 5. Long wind farm wakes observed behind Belwind1 and Thornton Bank from RADARSAT-2 intensity map (left) and wind speed map (right).

At DTU Wind Energy the WRF mesoscale model [7] has been used to model the divergence of the wakes induced by the Belwind1 and Thornton Bank wind farms. The challenge of wake modelling

with mesoscale models is the limited model's horizontal resolution. To avoid resolving the completely parametrized turbulence, the horizontal grid spacing, should be much larger than the turbulence length scale [11]. Consequently, the local turbine induced wake remains completely unresolved by the model and interaction takes place only between grid-cells. For the parametrization of the wind farms we use the Explicit Wake Parametrization (EWP) [12]. It applies a grid-cell averaged deceleration to the model's flow equation and additional turbulence is produced by the Planetary Boundary Layer (PBL) scheme from the changed vertical shear in horizontal velocity. This renders the EWP parametrization PBL-scheme independent.

For the simulation we use WRF V3.4. The model was set-up with two nests inside the most outer domain I, which is driven by ERA-Interim reanalysis data [13]. The horizontal resolution is for the three domains 18, 6 and 2 km, respectively. The most inner (most expensive) nest is run twice, without and with the wind farm parametrization. The number of vertical layers is set to 60, with around 30 layers in the first 600 m. The second mass level is at around 12 m above sea level and is used for the comparison to the satellite images. The PBL-Scheme with the second order closure Mellor-Yamada-Nakanishi-Niino (MYNN) [14] was used. For completeness we summarized the most important physics parametrizations and nudging options used: Convection [15] (Domain I and II) and microphysics [16], long wave radiation [17], shortwave radiation [18], surface scheme [19] and nudging of U and V Domain I outside the PBL.

The most inner domain extends 262 by 208 grid-cells in the west-to-east and south-to-north direction, respectively. The simulation period is three days, starting at the 29th of June. Figure 6 shows the simulated normalized velocity and the velocity deficit at 10m above sea level (ASL) over the sea surface only.

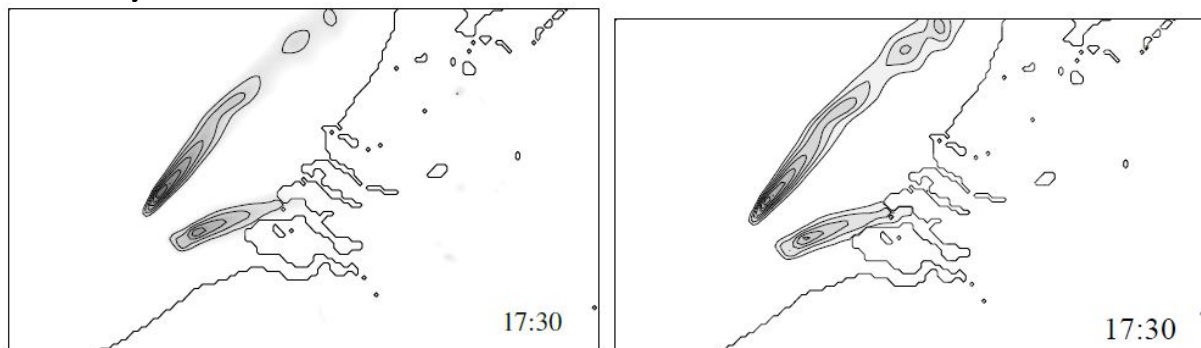


Figure 6. WRF model results on wind farm wakes behind Belwind1 and Thornton Bank: (left) normalized velocity at 10m ASL with velocity contours in ranges from 0.8 to 0.99; (right) velocity deficit at 10m ASL with contours in ranges from -1.25 to -0.1 ms^{-1} over the sea surface only.

From the satellite image (Figure 5) a clear wake of around 70 km long behind the Thornton Bank wind farm is found and the wake behind the Belwind1 wind farm appears to be even longer. Besides a bending, also a divergence of the wakes can be noticed. Similar features can be found in Figure 6 from WRF. Compared to the satellite image the wake's orientation is somewhat too far to the south in the model simulation. The wake interacts with the Dutch island Schouwen-Duiveland instead of with the most northerly delta island Goeree-Overakkee. Furthermore, the simulations show an even bigger divergence of the two wakes compared to that from the satellite image. Also the Belwind1 wind farm wake, when referring to the most outer contours of -0.1 ms^{-1} , seems to extend further compared to the satellite image. However, the considered deficit is very small and perhaps not visible in the satellite image.

The wind farm induced wakes from the satellite images include mesoscale features, such as a divergence of wakes from two nearby wind farms and are also the result of unsteady flow conditions. In this section we compared the satellite images visually to a velocity deficit obtained from a WRF simulation without wind farm to one with wind farms parametrized with the EWP scheme. The results show that the mesoscale model can capture the mesoscale features. However, we cannot expect the “snap-shots” of the WRF simulations to match the observed velocity and wind directions in the SAR images perfectly. Therefore, the results for single events should be used qualitatively and a quantitative comparison could be made from statistics over longer periods.

4. Wake case at alpha ventus and Horns Rev-1/-2 with long wakes

The RADARSAT-1 image is acquired on 15th August 2012 at 05:49:27 UTC. There are long wind farm wakes observed at alpha ventus and Horns Rev-1/-2 and less visible wakes behind Bard Offshore, see Figure 7. The wind direction is from the southeast. The corresponding SAR wind retrieval maps covering the Horns Rev and alpha ventus wind farms are also shown in Figure 7. The free stream wind velocity is around 7 ms^{-1} while the wake region has winds 5 ms^{-1} .

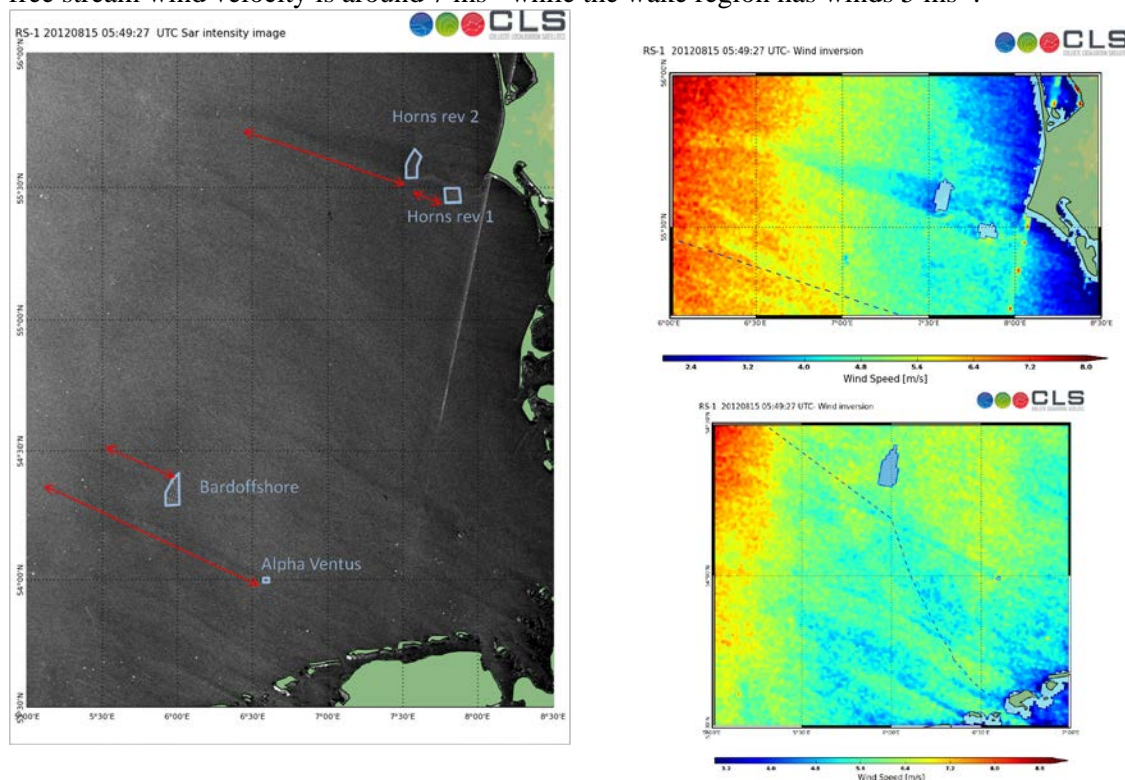


Figure 7. Long wind farm wakes observed behind alpha ventus, Horns Rev-1/-2 and too lesser extend BARD Offshore from RADARSAT-1 intensity map (left) and wind speed at Horns Rev-1/-2 (upper left) and alpha ventus (lower left).

At CENER the WRF model, version 3.4 [7] is configured using 4, two-way nested domains with resolutions of 10km, 3.33km, 1.11km and 370m with 35 vertical levels spreading from the surface until the top of the atmosphere. The domain is centred at 54.01°N , 6.606°E with sizes 250×250 , 268×2688 , 286×286 and 328×328 . The simulation is driven by GFS 12UTC input data which have a

horizontal resolution of 0.5° by 0.5° . The physics parameterizations used are: Microphysics (WRF Single-Moment (WSM) [20]); Long wave radiation (Rapid Radiative Transfer Model [17]); Shortwave radiation (Dudhia scheme [18]); Surface layer MYNN [14], Land surface (Noah [19]), PBL (MYNN 2.5 level TKE scheme [14]) and Cumulus (Kain-Fritsch (new Eta) [21]).

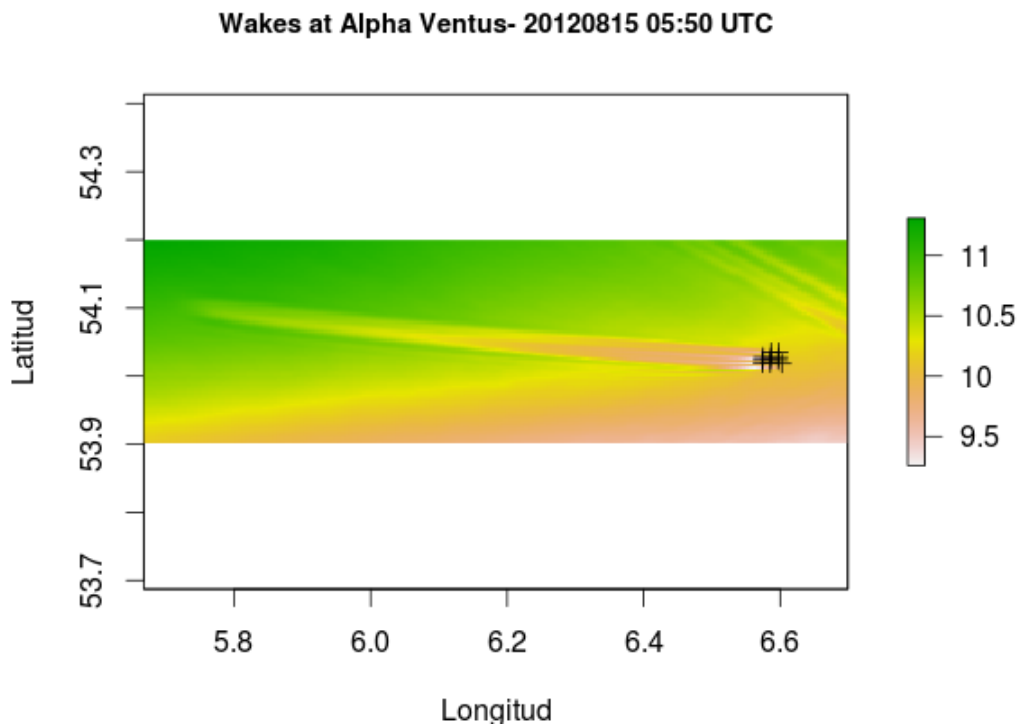
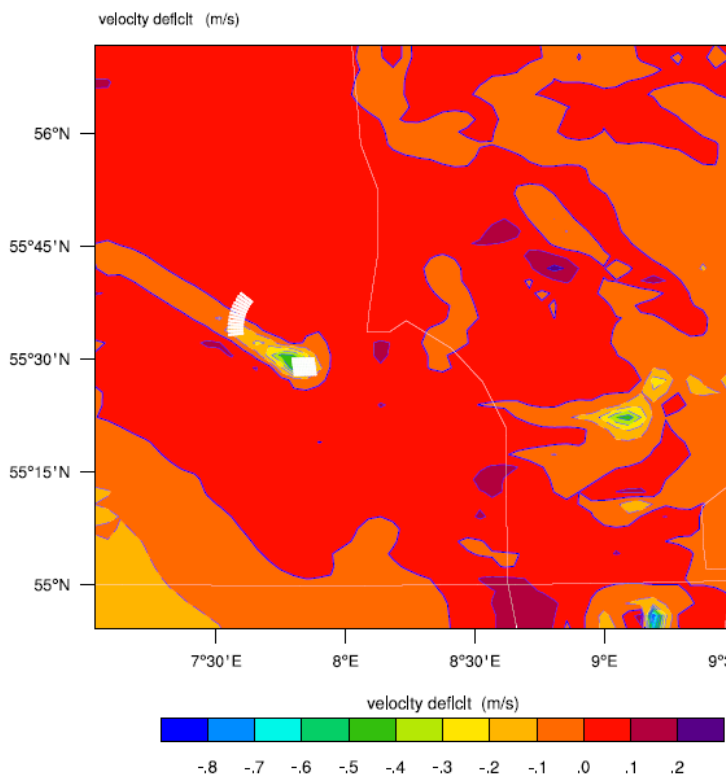


Figure 8. Wind farm wake modelled by WRF at alpha ventus with wind speed scale in ms^{-1} .

A very clear wake is visible stretching for several kilometres behind the alpha ventus wind farm in Figure 8 as modelled in WRF. In this case, the simulated wake seems to be able to emulate both shape and direction of the observed wake. The output from the mesoscale model can only be visually compared with the satellite images that correspond to the same situation. The result is useful as a first approach to the development of a robust methodology to predict or simulate the effects on wind speed of neighbouring offshore wind farms in an area of interest.

The Horns Rev-1/-2 wind farm wake has been investigated by CIEMAT using WRF. The WRF model (version 3.4) [7] has been configured using a total of five two-way domains interacting with a three to one spatial refinement in order to reach a horizontal resolution of 333 m in the innermost domain that comprises the Horns Rev wind farm. We prescribed a total of 36 vertical levels, five of them within the first 200 m of the atmosphere. The five domains used in the WRF simulation with 27,000, 9000, 3000, 1000 and 333 m of horizontal resolution. The number of points (west-east by north-south) for each one of the five domains are 70x65, 49x49, 58x49, 43x43, and 43x43. Usually, each simulation consists of a sequence of short runs of the model. In each set of runs, the model is initialized at 0 UTC every day and run for 48 h storing the output every hour. The first day is discarded as a spin up of the

model, whereas the output for the second day is retained as the simulation for that day. The initial and boundary conditions necessary to run the mesoscale model come from the ERA-Interim reanalysis project [22]. In this particular case, as the goal is to get the instantaneous WRF output to compare to the SAR image of the wake, the model is initialized the day before. A number of sub-grid scale processes are parameterized by WRF. The shortwave and longwave radiation schemes follow the works by [18] and [17] respectively. Microphysical processes are represented with the WRF single-moment six class scheme [20], whereas the cumulus effects are parameterized only in the outermost three domains [14, 23]. The air-sea momentum flux is parameterized following the work by Charnock. The effects of the turbulent vertical mixing within the planetary boundary layer are parameterized using a 1.5 order scheme that predicts the turbulent kinetic energy [14] and advects it with the wind. The scheme is based on the work by Mellor and Yamada [25] but includes a better formulation of buoyancy effects and a master length scale that depends on atmospheric stability. The effects of the wind turbines over the atmospheric flow are parameterized following the work by [26].



The wind turbines are represented as an elevated sink of momentum and a source of turbulent kinetic energy that responds to the wind speed according to a specified function approximating the effects of the turning rotors on the flow. The scheme is comprehensively documented in the work by [26]. This method has been shown to produce a realistic representation of wind farm wakes [20, 26] but a comprehensive evaluation of its performance has not been performed yet.

In order to obtain the wind speed deficit, that is plotted to compare with the satellite wake images, the WRF model is run twice, the first one without the wind farm (Horns Rev I), and the second one with the wind farm inside. The result is shown in Figure 9. The wake shape is very similar to the one on the satellite image.

Figure 9. Wind farm wake modelled by WRF at Horns Rev-1/-2 showing velocity deficit in ms^{-1} near the time of satellite observation on 15 August 2012.

5. Summary and conclusion

The simulations performed by the micro- and meso-scale models tried to reproduce the real effects of several wind farms on the downstream wind observed through SAR satellite images. In some of the

satellite observations, clearly wakes were visible stretching for dozens of kilometres, which by itself is a proof of the importance of this type of phenomena. Only qualitative comparison is possible.

The wind farm parameterization used by the WRF mesoscale model could provide a useful tool when studying the effects of a single or cluster of wind farms on the wind speed in a neighbouring area. The simulated wakes seem to emulate fairly well the shape and directions of the observed ones, but there is still room for improvement. The final goal is to obtain estimation of the expected wind speed deficit on an area of interest by the surrounding operating or planned wind farms. This estimation could constitute a decisive factor when deciding the layout or location of a new wind farm, or in the prediction of expected losses on wind energy production. In order to accomplish this final goal, measurements of wind speed or production in operating offshore wind farms would be crucial in order to properly calibrate the current state of the art mesoscale models.

Acknowledgments

Support from the EERA DTOC project FP7-ENERGY-2011-1/ n°282797 and satellite images from RADARSAT-1/-2 from Data and Products © MacDonald, Dettewiler and Associates Ltd are acknowledged.

References

- [1] Christiansen M B and Hasager C B 2005 *Wake effects of large offshore wind farms identified from satellite SAR*. Remote Sens. Environ. v. 98 p. 251-268
- [2] Christiansen M B and Hasager C B 2006 *Using airborne and satellite SAR for wake mapping offshore*. Wind Energy v. 9 p. 437-455
- [3] Li X and Lehner S 2013 *Observation of TerraSAR-X for Studies on Offshore Wind Turbine Wake in Near and Far Fields*. IEEE Journal of Selected Topics in Applied Earth Observations and Remote Sensing 05/2013; 6(3).
- [4] Longépé N, Hajduch G, Pelich R, Habonneau J and Lebras, J-Y 2013 *SAR-based Ship Monitoring: Advanced Methodologies with Medium Resolution Images (from WSM ASAR to EWS/IWS S1 Mission)*. ESA Living Planet Symposium, 9-13 September 2013, Edinburgh, United Kingdom.
- [5] Dagestad K-F, Horstmann J, Mouche A, Perrie W, Shen H, Zhang B, Li X, Monaldo F, Pichel W, Lehner S, Badger M, Hasager C B, Furevik B, Foster R C, Falchetti S, Caruso M J and Vachon P 2013 *Wind retrieval from synthetic aperture radar - an overview*. Proceedings of SEASAR 2012, 4th SAR Oceanography Workshop (SEASAR 2012). Tromsø, Norway, 18-22 June 2013, ESA SP709, pp. 22.
- [6] Katic I, Højstrup J and Jensen N O 1986 *A simple model for cluster efficiency*. Proceedings of the European Wind Energy Association Conference & Exhibition. Rome, Italy
- [7] Skamarock W C, Klemp J B, Dudhia J, Gill D O, Barker D M, Duda M, Huang X Y, Wang W and Powers J G. 2008 *A description of the advanced research WRF version 3*. Technical Report TN-475+STR, NCAR, 2008. [WRF is a community model provided by the National Center for Atmospheric Research, Boulder CO, sponsored by the National Science Foundation].
- [8] Quilfen Y, Chapron B, Elfouhaily T, Katsaros K and Tournadre J 1998 *Observation of tropical cyclones by high-resolution scatterometry*, Journal of Geophysical Research, 103(C4), 7767–7786. doi:10.1029/97JC01911.
- [9] Mouche A, Hauser D, Daloze J-F and Guerin C 2005 *Dual-polarization measurements at C-band over the ocean: results from airborne radar observations and comparison with Envisat ASAR data*. IEEE Transactions on Geoscience and Remote Sensing, 43(4), 753-769. 10.1109/TGRS.2005.843951

- [10] Barthelmie R J, Badger J, Pryor S C, Hasager C B, Christiansen M B and Jørgensen B H 2007 *Offshore coastal wind speed gradients: Issues for the design and development of large offshore wind farms*. Wind Engineering, 31(6), 369-382.
- [11] Wyngaard J C 2004 *Toward Numerical Modeling in the Terra Incognita*. Mon. Weather Rev., 61:1816- 1826, 2004.
- [12] Volker P J H 2014 *Wake Effects of Large Offshore Wind Farms - a study of the Mesoscale Atmosphere*. DTU Wind Energy, Ph.D. Thesis, p.132, 2014.
- [13] Uppala S M, Kallberg P W, Simmons A J, Andrae U, da Costa, Bechtold V, Fiorino M, Gibson J K, Haseler J, Hernandez A, Kelly G A, Li X, Onogi K, Saarinen S, Sokka N, Allan R P, Andersson E, Arpe K, Balmaseda M A, Beljaars A C M, van de Berg L, Bidlot J, Bormann N, Caires S, Chevallier F, Dethof A, Dragosavac M, Fisher M, Fuentes M, Hagemann S, Holm E, Hoskins B J, Isaksen L, Janssen P A E M, Jenne R, McNally A P, Mahfouf J-F, Morcrette J-J, Rayner N A, Saunders RW, Simon P, Sterl A, Trenberth K E, Untch A, Vasiljevic D, Viterbo P and Woollen 2005 *The ERA-40 re-analysis*. Quart. J. R. Meteorol. Soc., 131, 2005
- [14] Nakanishi M and Niino H 2009 *Development of an improved turbulence closure model for the atmospheric boundary layer*. J of the Meteorol Soc of Japan, 87:895-912, 2009.
- [15] Kain J S 2004 *The Kain-Fritsch convective parameterization: An update*. J. Appl. Meteor., 43:170{181, 2004
- [16] Thompson G, Field P R, Rasmussen R M and Hall W D 2008 *Explicit forecasts of winter precipitation using an improved bulk micro- physics scheme. Part II: Implementation of a new snow parameterization*, Mon. Weather Rev., 136, 5095–5115, 2008
- [17] Mlaver E J, Taubman S J, Brown P D, Iacono M J and Clough S A 1997 *Radiative transfer for inhomogeneous atmosphere: RRTM, a validated corrected-k model for the long wave*. J. Geophys. Res., 102:16663{16682, 1997.
- [18] Dudhia J 1989 *Numerical study of convection observed during the wind monsoon experiment using a mesoscale two-dimensional model*. J. Atmos. Sci., 46:3077{3107, 1989.
- [19] Chen F and Dudhia J 2001 *Coupling an advanced land-surface/ hydrology model with the Penn State/ NCAR MM5 modeling system. Part I: Model description and implementation*. Mon. Wea. Rev., 129:569{585 , 2001
- [20] Hong S Y, Noh Y and Dudhia J 2006 *A new vertical diffusion package with an explicit treatment of entrainment processes*. Monthly Weather Review 2006; 134: 2318–2341.
- [21] Kain J S and Fritsch J M 1990 *A one-dimensional entraining/detraining plume model and its application in convective parameterization*, Journal of the Atmospheric Sciences, vol. 47, no. 23, pp. 2784–2802
- [22] Dee D P, Uppala S M, Simmons A J, Berrisford P, Poli P, Kobayashi S, Andrae U, Balmaseda M A, Balsamo G, Bauer P, Bechtold P, Beljaars A C M, van de Berg L, Bidlot J, Bormann N, Delsol C, Dragani R, Fuentes M, Geer A J, Haimberger L, Healy S B, Hersbach H, Hólm E V, Isaksen L, Kallberg P, Köhler M, Matricardi M, McNally A P, Monge-Sanz B M, Morcrette J-J, Park B-K, Peubey C, de Rosnay P, Tavolato C, Thépaut J-N and Vitart F 2011 *The Wind Energ.* (2014) © 2014 John Wiley & Sons, Ltd. DOI: 10.1002/we
- [23] Kain J S and Fritsch J M 1990 *A one-dimensional entraining/detraining plume model and its application in convective parameterization*. J of Atmospheric Sciences 1990; 47: 2784–2802.
- [24] Kain J S and Fritsch J M 1993 *Convective Parameterization for Mesoscale Models: The Kain-Fritsch Scheme. The Representation of Cumulus Convection in Numerical Models*, Meteor. Monogr., No. 24. American Meteorological Society: Boston, 1993. pp. 165–170.
- [25] Mellor G L and Yamada T 1982 *Development of a turbulence closure model for geophysical fluid problems*. Reviews of Geophysics and Space Physics 1982; 20: 851–875.
- [26] Fitch A C, Lundquist J K and Olson J B 2013 *Mesoscale influences of wind farms throughout a diurnal cycle*. Monthly Weather Review 2013; 141: 2173–2198.